Mechatronics 21 (2011) 1043–1054

Contents lists available at ScienceDirect

Mechatronics

journal homepage: www.elsevier.com/locate/mechatronics

Geared PM coreless motor modelling for driver's force feedback in steer-by-wire systems

Roland Pastorino *, Miguel A. Naya, José A. Pérez, Javier Cuadrado

Mechanical Engineering Laboratory, University of La Coruña, Escuela Politécnica Superior, Mendizábal s/n, 15403 Ferrol, Spain

ARTICLE INFO

Article history:
Received 29 March 2010
Accepted 4 May 2011
Available online 13 July 2011

Keywords:
Geared PMDC motor model
Steering wheel system model
Bristle friction model
Gearbox elasticity
Backlash modelling
Steer-by-wire system

ABSTRACT

Gearboxes allow for changes in the motor's torque and speed ranges, thus allowing the motor to function at its best operation ranges. As a consequence, smaller and low cost motors can be used in comparison with direct drive motors. Nevertheless, gearboxes introduce nonlinearities to the system such as friction, backlash and flexibility. When geared motors are employed, a controller using a torque sensor or a torque observer is normally required to compensate for the drawbacks associated with the gearbox and the servo-amplifier. The design of such a controller requires the comprehensive knowledge of the system's dynamics. In this paper, a general approach to model accurately amplifier–motor–gearbox assemblies has been developed. This approach that takes into account backlash, flexibility, friction for stiction and sliding, identification procedures, is applicable to a wide range of amplifier–motor–gearbox assemblies. It is explained by applying it to a particular case: an amplifier–motor–gearbox assembly for a driver's force feedback system. In the design of driver's force feedback systems for steer-by-wire systems or for high fidelity Human in the Loop (HiL) driving simulators, either direct drive motors or geared motors are used, independently of the motor type. The assembly considered here is composed of a two stage planetary gearbox, a coreless PMDC motor and a linear four quadrant servo-amplifier. It is installed in an X-by-wire (XBW) vehicle prototype, Both the amplifier and the mechanical components were built in the model. The four quadrant operating modes of the amplifier were taken into account. Friction within both the motor and the gearbox are modelled using a modification of the LuGre friction model that allows friction to be considered as load-dependent. Backlash and flexibility in the gearbox are considered together using a fifth order polynomial for each rotational direction. The identification procedures necessary to calculate the parameters of the model are presented. Because all the parameters of the model have a direct physical significance, these identification procedures are easy to realize. Comparisons between simulations realized with Simulink and the experimental data for three typical driving situations show that the model is highly accurate at representing real system dynamics.

1. Introduction

Gearboxes allow for changes in the motor's torque and speed ranges, thus allowing the motor to function at its best operation ranges. As a consequence, smaller and low cost motors can be used in comparison with direct drive motors. Nevertheless, the use of gearboxes has several drawbacks such as friction, backlash, flexibility or additional inertia. To avoid oversized direct drive motors, whilst maintaining good dynamic performances, the use of geared motors requires to compensate for the previously mentioned disadvantages. A controller using a torque sensor or a torque observer is normally required to compensate for the drawbacks associated with the gearbox and the servo-amplifier. The design of such a controller requires the comprehensive knowledge of the system's dynamics.

Friction, backlash and flexibility have previously been studied separately [1–4], more rarely together. Friction and backlash were treated together in Refs. [5,6] and friction and flexibility in Ref. [7]. Inertia is commonly taken into account in the control loop. In this paper, a general approach to model accurately amplifier–motor–gearbox assemblies has been developed. This approach that takes into account backlash, flexibility, friction for stiction and sliding, identification procedures, is applicable to a wide range of amplifier–motor–gearbox assemblies. It is explained by applying it to a particular case: an amplifier–motor–gearbox assembly for a driver's force feedback system of a SBW system.

Steer-by-wire (SBW) systems form part of the recent by-wire technology that is being developed in the automotive industry. SBW systems have no mechanical linkage (steering column) between the steering wheel and the rack and pinion gear system.

* Corresponding author.
E-mail address: rpastorino@udc.es (R. Pastorino).

0957-4158/$ - see front matter © 2011 Elsevier Ltd. All rights reserved.
doi:10.1016/j.mechatronics.2011.05.006

Therefore the steering task is performed by two electrical motors. The first, the road wheel motor (RwM) steers the front wheels of the vehicle following the angular position of the steering wheel. The second motor, called the steering wheel motor (SwM), is responsible for generating a reaction torque to the steering wheel. This is the driver's force feedback motor. SBW systems have several advantages over conventional automotive steering systems. Undoubtedly, the most significant of these is active steering capability, the ability to tune the driver's steering input thus improving vehicle stability and manoeuvrability. Another significant advantage is the freedom to modify the steering wheel torque through driver's feedback control.

SBW systems are widely used in both vehicle prototypes and vehicle simulators. Although SBW systems allow for a wide range of actuator choices, the use of brushless (electronically commutated) motors appears to be the most commonly used. This wide range of actuator choices is reflected in previous research studies. For example, a brushed DC servomotor with a timing belt was selected in Ref. [8] as the SwM. In Ref. [9], the SwM is a Permanent Magnet (PM) synchronous motor in direct drive. The SwM in Ref. [10] is a direct drive brushless actuator. Another choice of SwM actuator could be a brushless DC motor coupled with a harmonic-drive gear [11] or a worm gear [12]. In Ref. [13], the driver's torque feedback system is equipped with a gear set and two AC brushless actuators for redundancy in case of system fault. A disturbance observer is employed in Ref. [14] to estimate the torque in the steering wheel using a brushless synchronous motor and two encoders. Brushless motors are appreciated for their high efficiency, their small size, their low maintenance and even for the high heat capacity of their stators that allows for longer overload time. Despite their superior qualities, brushless motors are less commonly used than brushed types in motion-control applications, mainly due to their higher price.

When designing a SBW system, the choice between a direct drive motor and a geared motor for the SwM is based on a compromise in the motor dimensioning. Selecting a direct drive motor implies a bigger motor size than for a geared motor. Therefore, here, the use of a direct drive motor would imply a high electrical consumption. In this project, a SBW system using geared coreless DC motors has been installed in an X-by-wire (XBW) vehicle prototype. The combination of gearboxes and coreless DC motors guarantees low cost SBW systems. The coreless (or ironless) motors are PM brushed DC motors. They have no iron core, therefore no iron losses, low friction and an acceptable level of thermal dissipation. The design of a low-inertia rotor is the key here to rapid acceleration and fast reaction time. Thus coreless motors appear to be a possible low-cost option when designing a SBW system. Precision planetary gearboxes, i.e. with a low backlash angle, are used to increase motor's torque.

This paper is organized as follows: in Section 2, the implemented SBW system is described. The model of the driver's force feedback system is presented in Section 3. The parameters of this model are identified for three different operating modes of the steering wheel system in Section 4. Finally, concluding remarks are presented in Section 5.

2. The driver's torque feedback of the SBW system

2.1. The complete SBW system

Fig. 1 shows the block schematic of the complete SBW system that has been installed in the XBW vehicle prototype. This SBW system is composed of two identical geared DC motors, three encoders, a torque sensor and an electrical current sensor. With respect to the rack system, the torque sensor has a range of ±17 Nm and the encoder "A" has a resolution of 0.18° (500CPR). The specifications of the coreless DC motors (M66CI 500 L-24, KMclennan, UK) are compiled together in Table A.1. The specifications of the driver's force feedback system are described in Section 2.2.

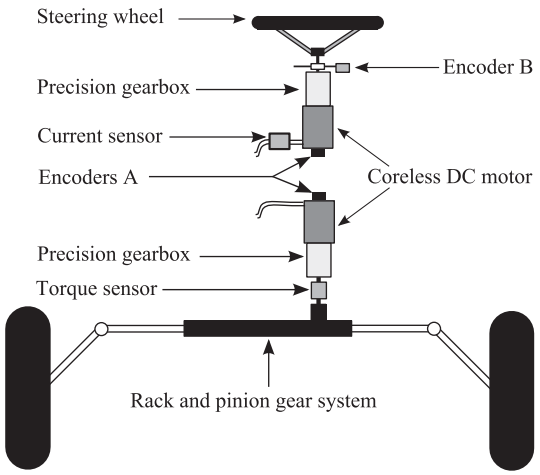

Fig. 1. Steer-by-wire system.

The gearboxes are high strength and have a two stage planetary construction (IP57-M02, Mclennan, UK). The backlash angle is small ($\leqslant 0.5°$) and the gearbox ratio is 50 (ω_{in}/ω_{out}).

2.2. The driver's force feedback system

Fig. 2 shows the CAD assembly of the driver's force feedback system and Fig. 3 shows the block schematic. Since the output shaft of the gearbox turns fifty times slower than the shaft of the motor, encoder "B" must have a higher resolution (0.0036° or 2500 CPR) than encoder "A". The DC motor is powered by a 24 VDC battery through a four quadrant linear amplifier (MSE421, Mclennan, UK) that is used as a torque controller. In this control mode, the maximum motor torque is of ±12 Nm. This voltage range has been chosen to match a subvoltage range of any electrical car batteries. Moreover this allows to employ common low-cost amplifiers. A data acquisition processor (DAP) is used to send the reference current command to the amplifier. The DAP (DAP

Fig. 2. Driver's force feedback system.

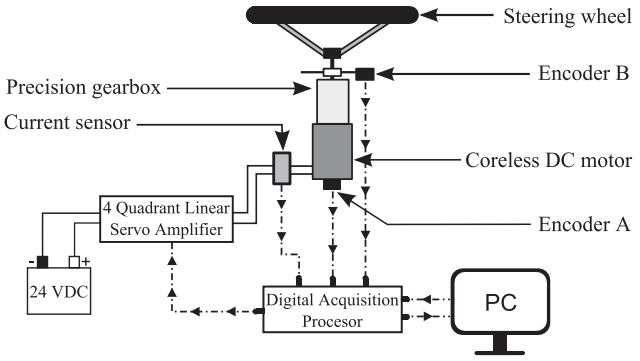

Fig. 3. Detailed driver's force feedback system.

4200a, Microstar Laboratories, USA) and its corresponding expansion boards sample sensor information, control the servoamplifier and communicate with the PC for user interface update. As mentioned before, since the gearbox introduces nonlinearities (friction, backlash, flexibility) into the system, the torque in the steering wheel fails to match the reference torque that is sent by the DAP to the servoamplifier. This problem especially appears in the transient. Consequently, the driver does not receive always an accurate feedback torque. This problem may be solved by installing a sensor torque between the gearbox and the steering wheel [11]. However this solution implies that additional elasticity is introduced into the mechanical system thus degrading the system performance. Moreover, the stability of force sensing could be improved by replacing the torque sensor with a reaction torque observer [15].

To further understand the system dynamics, the following section illustrates a high performance model of the steering wheel system built in Simulink.

3. Driver's force feedback system model

3.1. System modelling

The model of the driver's force feedback system presented in Fig. 4 is composed, as in the real system, of four parts: the four quadrant linear amplifier, the motor, the gearbox and the steering wheel. Each one of these parts is described below.

3.1.1. Amplifier model

The amplifier is modelled as a current controller which takes into account the four quadrant operating modes. The dynamics of the PI controller have been neglected since they are much faster than the dynamics of the rest of the model. First the current reference given by the digital acquisition processor, i_{dap}, is bounded by the two values i_{sat}^- and i_{sat}^+ defining the reference current i_{ref} as can be seen in Eq. (1). These saturation limits are considered constant despite their time fluctuations.

$$i_{ref} = \begin{cases} i_{sat}^+ & \text{if } i_{sat}^+ \leqslant i_{dap} \\ i_{dap} & \text{if } i_{sat}^- \leqslant i_{dap} \leqslant i_{sat}^+ \\ i_{sat}^- & \text{if } i_{dap} < i_{sat}^- \end{cases} \tag{1}$$

Next, the voltage of the motor, V_a, is calculated using Eq. (2) or Eq. (3) depending on the sign of i_{ref}. Both equations have the same physical interpretation hence only Eq. (2) is discussed. In this equation, the amplifier changes the voltage to attempt to maintain i_a equal to i_{ref}, the motor's current. When $i_{ref} < i_a$, as shown in Eq. (2a), the amplifier decreases the motor's voltage on the base of the difference between the motor's current i_a and the reference current i_{ref} multiplied by the constant k_1. Then, in Eq. (2b), when $0 < i_a \leqslant i_{ref}$, the amplifier sets the voltage to its maximum value, V_{sat}^+. Finally, when i_{ref} and i_a have different signs, the amplifier increases the motor's voltage above its maximum value V_{sat}^+ by a factor using the motor's current i_a and a constant k_2, Eq. (2c). All the values of the amplifier coefficients are given in Table C.1.

If $i_{ref} \geqslant 0$

$$V_a = \begin{cases} V_{sat}^+ - k_1 \cdot (i_a - i_{ref}) & \text{if } i_{ref} < i_a \quad \text{(a)} \\ V_{sat}^+ & \text{if } 0 < i_a \leqslant i_{ref} \quad \text{(b)} \\ V_{sat}^+ - k_2 \cdot i_a & \text{if } i_a \leqslant 0 \quad \text{(c)} \end{cases} \tag{2}$$

If $i_{ref} < 0$

$$V_a = \begin{cases} V_{sat}^- - k_1 \cdot (i_a - i_{ref}) & \text{if } i_a < i_{ref} \quad \text{(a)} \\ V_{sat}^- & \text{if } i_{ref} \leqslant i_a < 0 \quad \text{(b)} \\ V_{sat}^- - k_2 \cdot i_a & \text{if } i_a \geqslant 0 \quad \text{(c)} \end{cases} \tag{3}$$

3.1.2. DC motor model

The DC motor is modelled as a rigid body with inertia J_m. The friction torque τ_{fm} models the friction between the shaft and the armature as well as the friction between the inner gears of the first stage and the ring gear of the two stage planetary gearbox. The friction model is later explained in Section 3.2.1. The motor shaft elasticity has been included in the gearbox elasticity. The mathematical equation of the PMDC motor is shown in the following equation:

$$V_a = R_a \cdot i_a + L_a \cdot \frac{di_a}{dt} + k_v \cdot \omega_m \tag{4}$$

where V_a is the supply voltage to the armature (V), R_a is the resistance of the armature winding (Ω), L_a is the leakage inductance in the armature winding (H), k_v is the motor voltage constant (V/rad/s), ω_m is the motor angular velocity (rad/s) and i_a is the armature current (A). Finally, the motor's torque τ_m is directly obtained from the motor's current i_a as stated in the following equation:

$$\tau_m = k_m \cdot i_a \tag{5}$$

where k_m, the motor torque constant, is given in Table A.1. The Simulink model of the DC motor is shown in Fig. 5.

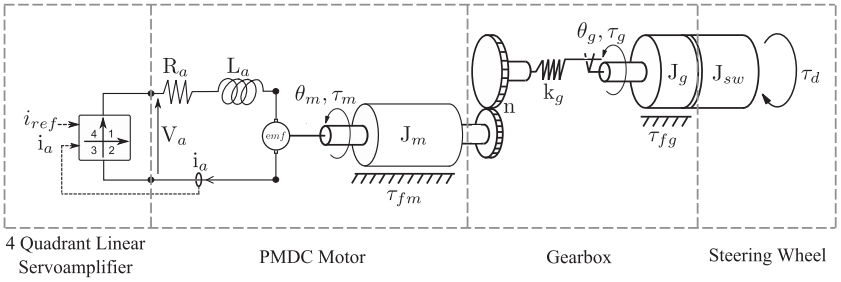

Fig. 4. Schematic of the driver's force feedback system.

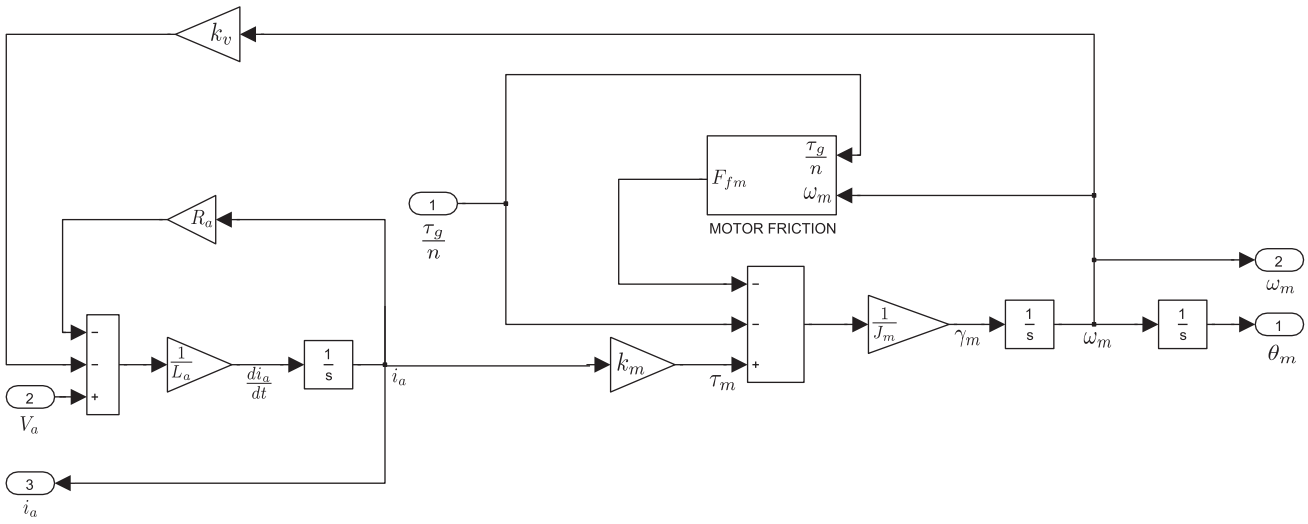

Fig. 5. Simulink model of the DC motor.

3.1.3. Gearbox model

At first approximation, as in Ref. [11], gearbox elasticity is often considered proportional to the twist of the gearbox, θ_a, as stated in Eq. (7). Nevertheless, Wernholt and Gunnarsson [7] modelled the elasticity of their gearbox by adding a cubic term to the proportional term. If backlash (or gear play) has to be taken into account, the most common models used are the dead zone model and the backlash exact model as explained in Ref. [1]. Although these backlash models clearly represent the extent of backlash between two gears, they are less accurate when used with a higher number of gears, as is the case here with the two stage planetary gearbox. In practice, within such a gearbox, there are numerous clearances and, due to gear friction, backlash is not so accurately marked. One way to take backlash into account when using multiple gears is to model the gearbox elasticity and the backlash together as follows. Here, the relation between the twist of the gearbox and the elastic term of the gearbox torque $\tau_{g\_elastic}$ is modelled by adding to the proportional term, a cubic term and another to the fifth power, as shown in Eq. (6). Only the odd power terms are considered in order to maintain the monotonically increasing shape for positive twist angle and the monotonically decreasing shape for negative twist angle of the backlash–flexibility curve.

$$\tau_{g\_elastic} = \begin{cases} k_{g1}^{+} \cdot \theta_a + k_{g3}^{+} \cdot \theta_a^3 + k_{g5}^{+} \cdot \theta_a^5 & \text{if } \theta_a > 0 \\ k_{g1}^{-} \cdot \theta_a + k_{g3}^{-} \cdot \theta_a^3 + k_{g5}^{-} \cdot \theta_a^5 & \text{if } \theta_a < 0 \end{cases} \tag{6}$$

$$\theta_a = \left(\frac{\theta_m}{n} - \theta_g\right) \tag{7}$$

where k_{g1}^{+}, k_{g3}^{+}, k_{g5}^{+}, k_{g1}^{-}, k_{g3}^{-}, k_{g5}^{-} are constant parameters, θ_m is the motor angle, n is the gearbox ratio (ω_{in}/ω_{out}), θ_g is the gearbox angle and θ_a is the twist of the gearbox. One advantage of modelling the elasticity and the backlash together is that the backlash angle is not required as in other models. Later, a viscous term τ_{g_visc} depending on the velocity of the twist angle $\dot{\theta}_a$ is added according to the following equation:

$$\tau_{g\_visc} = b_g \cdot \dot{\theta}_a \tag{8}$$

where b_g is a constant parameter whose value is given in Table C.3. Therefore the gearbox torque τ_g is the sum of the elastic and viscous terms as stated in the following equation:

$$\tau_g = \tau_{g\_elastic} + \tau_{g\_visc} \tag{9}$$

To complete the gearbox model, a friction torque τ_{fg} models the friction between the inner gears of the second stage and the ring gear of the two stage planetary gearbox. The friction model used is explained below in Section 3.2.1. The Simulink model of the gearbox is shown in Fig. 6.

3.1.4. System equations

The dynamics of the system are described by Eqs. (10) and (11) corresponding respectively to the dynamics of the motor and the gearbox.

$$\tau_m - J_m \cdot \ddot{\theta}_m - \tau_{fm} - \frac{\tau_g}{n} = 0 \tag{10}$$

$$\tau_g - J_{tot} \cdot \ddot{\theta}_g - \tau_{fg} + \tau_d = 0 \tag{11}$$

where $J_{tot} = J_g + J_{sw}$, J_m is the motor inertia, J_{sw} is the steering wheel inertia, J_g is the gearbox inertia, τ_d is the driver torque acting on the steering wheel, τ_{fm} is the motor friction torque, τ_{fg} is the gearbox friction torque and τ_g is the output torque of the gearbox. The remaining parameters have been defined previously.

3.2. Friction model and friction parameter identification

3.2.1. Friction model

Simple friction models that only account for a relation between velocity and friction force are in this case not suitable, as they do not consider the presliding behaviour, resulting in simulation errors at motion stops and reversals. For these models, at zero velocity, the friction force is constant: zero or F_s (F_c if F_s is not considered) instead of having a spring like behaviour. F_c is the Coulomb friction level and F_s is the level of the stiction force. That is why a bristle friction model, the LuGre model [3], is used. Some authors have proposed improvements of the latter, especially for the presliding behaviour [2]. Nonetheless, here, this behaviour is not crucial to such an extent that an improved LuGre model is necessary. The LuGre model has the following form:

$$\dot{z} = v - \sigma_0 \cdot \frac{|v|}{g(v)} \cdot z \tag{12}$$

$$g(v) = F_c + (F_s - F_c) \cdot e^{-(v/v_s)^2} \tag{13}$$

$$F = \sigma_0 \cdot z + \sigma_1 \cdot \dot{z} + \sigma_2 \cdot v \tag{14}$$

where v is the velocity, v_s is the Stribeck velocity, z is the average deflection of the bristles, σ_0 represents the stiffness of the bristles,

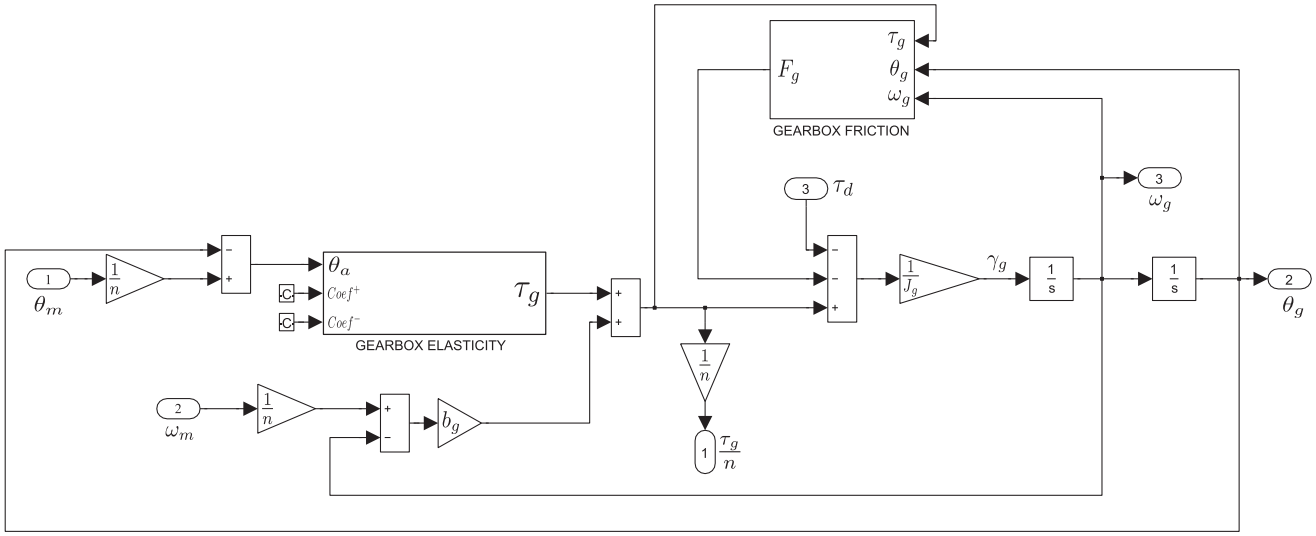

Fig. 6. Simulink model of the gearbox.

σ_1 is the damping coefficient of the bristles and σ_2 is the viscous damping.

Moreover, the friction in the gearbox appears in this case to be load-dependent. When the torque transmitted by the gearbox increases, the friction torque also increases. Load-dependent friction has previously been studied in only a few cases as in Ref. [16] where a load-dependent friction model is presented for a worm gear transmission. Here, the coulomb force, the stiction force and the viscous force are considered load-dependent. The load dependence is modelled as follows:

$$\begin{cases} F_c = \alpha_1 \cdot \sqrt{\tau_g} \\ F_s = \alpha_2 \cdot \sqrt{\tau_g} \\ \sigma_2 = \alpha_3 \cdot \sqrt{\tau_g} \end{cases} \quad \text{for the gearbox} \tag{15}$$

$$\begin{cases} F_c = \alpha'_1 \cdot \tau_g \\ F_s = \alpha'_2 \cdot \tau_g \\ \sigma_2 = \alpha'_3 \cdot \tau_g \end{cases} \quad \text{for the motor} \tag{16}$$

where $\alpha_1,\ \alpha_2,\ \alpha_3(\sqrt{\text{Nm}})$ and $\alpha'_1,\ \alpha'_2,\ \alpha'_3$ (dimensionless) are positive constants. The Simulink friction model of the DC motor is shown in Fig. 7. The friction model of the gearbox has exactly the same form.

3.2.2. Friction identification

To estimate some parameters of the LuGre model (F_s, F_c, v_s, σ_0, σ_1, σ_2), the shaft of the geared motor, with no load, is moved at several different speeds. During these tests, the speed is maintained constant in order to avoid exciting dynamic friction components. In this situation, the derivative of the average deflection of the bristles $\dot{z}$ is equal to zero and v is constant. Therefore Eq. (14) can written as shown in the following equation:

$$F = F_c + (F_s - F_c) \cdot e^{-(v/v_s)^2} + \sigma_2 \cdot v \tag{17}$$

The friction force is measured by means of motor current sensing. Measurements are recorded for 50 different constant speeds on each rotational direction, within a range of ±12,000°/s. The friction torque $\tau_{f,no\text{-}load}$ is obtained from the following equation:

$$\tau_{f,no\text{-}load} = k_{m,avg} \cdot i_{avg} \tag{18}$$

where i_{avg} is the average of the current drawn by the motor and $k_{m,avg}$ is the motor torque constant (Nm/A). The average value of $k_{m,avg}$ is given in Table A.1. As in a gearbox the friction is position dependent, the friction torque has an oscillatory behaviour depending on the position. Therefore the motor current is averaged over several turns before calculating the friction torque. After that, a

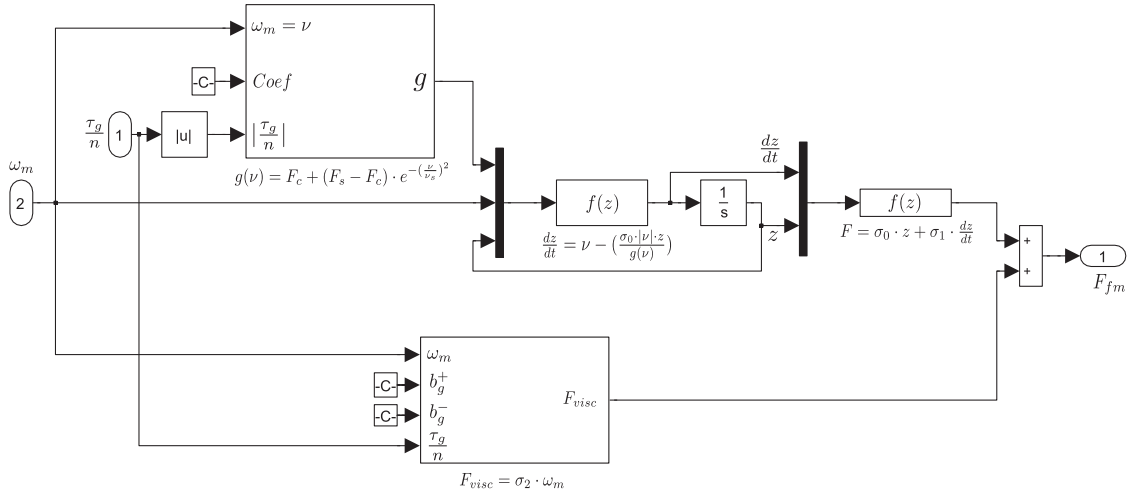

Fig. 7. Simulink model of the motor friction.

least-squares formulation is used to fit Eq. (17) to the experimental data. The least-squares method minimizes the summed square of residuals that is given by the following equation:

$$S = \sum_{i=1}^{n} (y_i - \hat{y}_i)^2 \tag{19}$$

where y_i is the experimental value and $\hat{y}_i$ is the fitted value. The experimental and model fitted friction curves are shown in Fig. 8.

The identified friction parameters are shown in Table B.1. These parameters do not correspond directly with τ_{fm} or τ_{fg} as the latter cannot be measured separately but they represent the sum $(\tau_{fm} + \tau_{fg})$ when the gearbox transmits zero torque. Therefore, these values only give the order of magnitude of the friction parameters. The bristle damping, represented by the coefficient σ_1, is neglected in the motor friction model as well as in the gearbox friction model, having verified with simulations that its contribution in this model is not significant. The remaining parameters $\sigma_{0,m}$, $\sigma_{0,g}$, α_1, α'_1, α_2, α'_2, $v_{s,g}$, $\sigma_{2,m}$ and $\sigma_{2,g}$ for each rotational direction were tuned to best fit the model to the experimental data, as is explained in Section 4. Further friction identification tests could be done, especially with the output shaft of the gearbox loaded during its movement. Nevertheless, as the friction parameters have a direct physical significance, their tuning to adjust the model to the experimental data has proved to be feasible and intuitive.

3.3. Gearbox elasticity and backlash identification

In order to identify the elasticity and backlash parameters, the gearbox output shaft is blocked with a torque sensor, as shown in Fig. 9. The motor torque is slowly ramped up and down on each rotational direction without stopping. Different maximum values for the motor torque are applied.

Fig. 10 shows the experimental data when the motor torque is ramped up and down on each rotational direction using full scale torque. The first observation is that this curve is not linear (as is usually supposed) and presents hysteresis. Actually, this hysteretic behaviour is due to the friction in the gearbox. The torque curve has an inflection point where, for low values of the twist angle, the torque transmitted by the gearbox is almost zero. This is the backlash zone (grey area). Finally the relation between the torque and the twist angle of the gearbox is approximated by two curves (positive and negative twist, solid lines without arrows) using Eq. (6). The coefficients for each rotational direction are shown in Table B.2.

At this point,the gearbox elasticity parameters are known. The few friction parameters that have been identified will be used as initial conditions for the optimization of all the friction parameters through comparisons between the experimental and the simulated data.

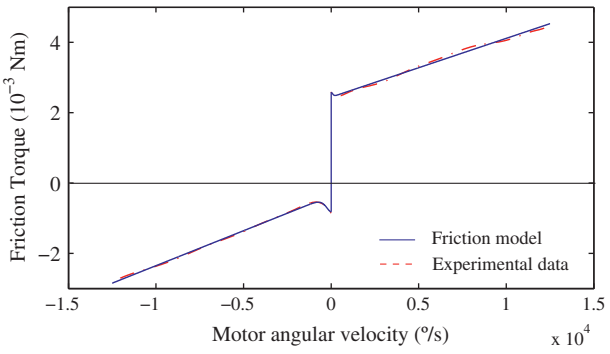

Fig. 8. No load friction curves.

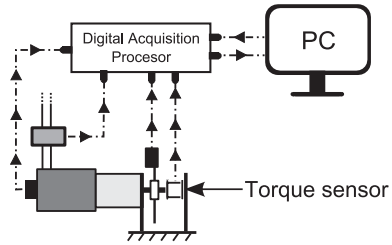

Fig. 9. Geared motor with the output shaft blocked.

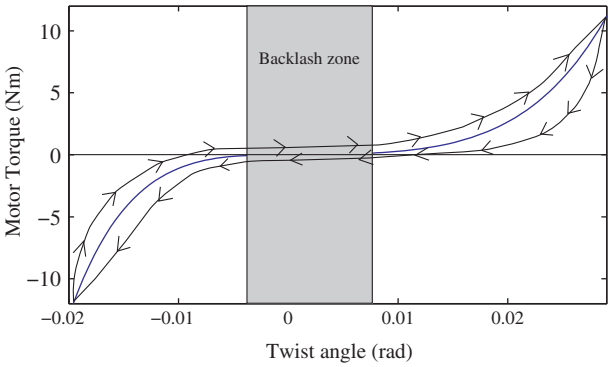

Fig. 10. Elasticity–backlash curve of the gearbox.

4. Identification procedures and simulation results for the driver's torque feedback system

In order to evaluate the accuracy of the model, three different tests corresponding to real situations are performed. In the first test, the steering wheel is blocked as though the driver were holding it tightly, preventing almost any rotation. In the second test, the driver leaves the steering wheel free and, in the third test, the driver holds and turns the steering wheel in both rotational directions while the motor is actuating. Table B.3 shows the inertia of different components forming part of the system. J_g is the sum of the gearbox inertia J_1 and the coupling inertia J_2. J_m is the inertia of the motor shaft, the sun gear and its adaptor. J_{sw} is the steering wheel inertia. Next, to quantify the accuracy of the model, a least mean square criterion is used, Eq. (19). Then the fit is obtained from the following equation:

$$Fit = 100 \cdot \left(1 - \frac{\sqrt{S}}{\sqrt{\sum_{i=1}^{N} (y(t) - \bar{y})^2}}\right) \tag{20}$$

where $y(t)$ is the measured output, $\bar{y}$ is the mean value of the measured output and S is the summed square of the residuals (see Eq. (19)).

4.1. Locked steering wheel

The first test is conducted with the steering wheel blocked, as shown in Fig. 9. In order to easily block the output shaft of the gearbox, the steering wheel is replaced by a torque sensor, fixed on one side, thus neglecting the steering wheel coupling elasticity. A scheme of the assembly is shown in Fig. 11, where k_s (=4500 Nm/rad) is the elasticity of the torque sensor.

The Simulink model of this assembly is shown in Fig. 12. Two different current commands are applied to the DC motor of the real system: a sine wave of period 1 s and a square wave of period 0.27 s. Three different amplitudes are tested: 1/3 of full scale

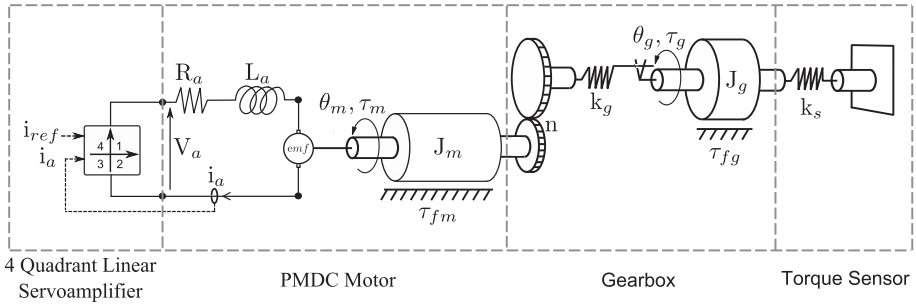

Fig. 11. Locked steering wheel system.

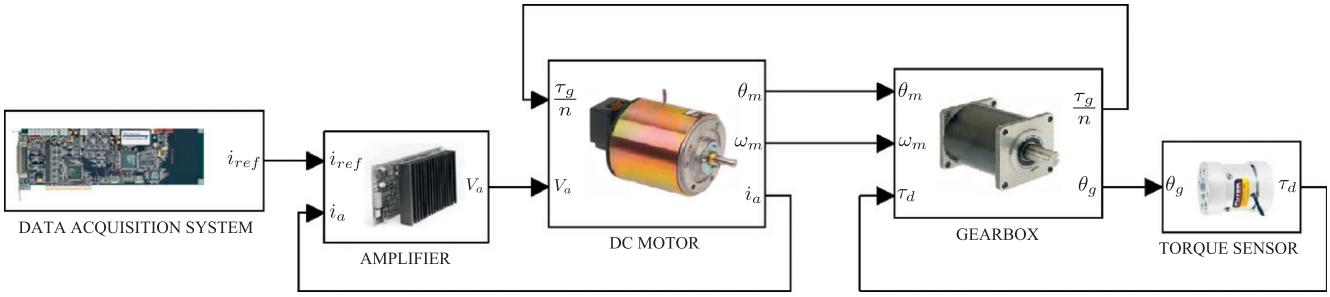

Fig. 12. Simulink model for the locked steering wheel system.

(0.14 Nm), 2/3 of full scale (0.28 Nm) and full scale (0.42 Nm). The amplitude of the steps of the square wave is randomly chosen (white noise distribution) within the selected amplitude. The period of the square wave is chosen so that the system has enough time to reach a steady state between two consecutive steps. The torque of the sensor is shown for a sine wave excitation in Fig. 13 and for a square wave excitation signal in Fig. 14.

These figures highlight several important characteristics of the real system. Fig. 13 shows the current saturation of the servoamplifier, the delay and the nonlinearities introduced by the gearbox. Fig. 14 shows the oscillatory behaviour of the system and especially the amplitude reached by the system with respect to the reference command. In order to adjust the model parameters that were either not identified or whose identification value is distant from the real value, several optimizations using comparison between experimental and simulated data are performed.

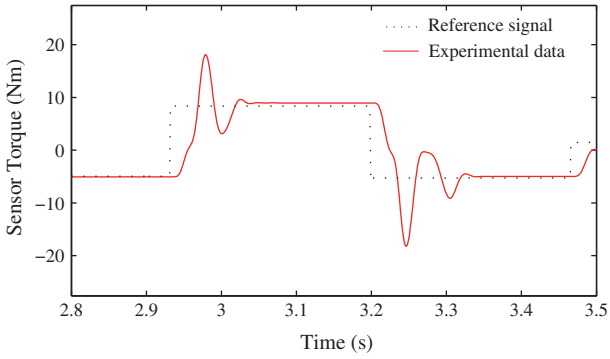

Fig. 14. Sensor torque, τ_d, for a square wave excitation signal.

4.1.1. Tuning of the amplifier parameters

The first parameters to be tuned are those of the amplifier. During the experiments, the current of the motor is recorded by means of the Hall effect sensor. The objective is to match the simulated current to the recorded current of the sensor. Both the model and the real system are excited with the same reference signal. The sine wave is used to adjust the saturation limits of the current. Fig. 15 shows the experimental and the simulated data for the sine wave reference. The fit, calculated using Eq. (20), between the experimental and the simulated velocity is of 96.8%.

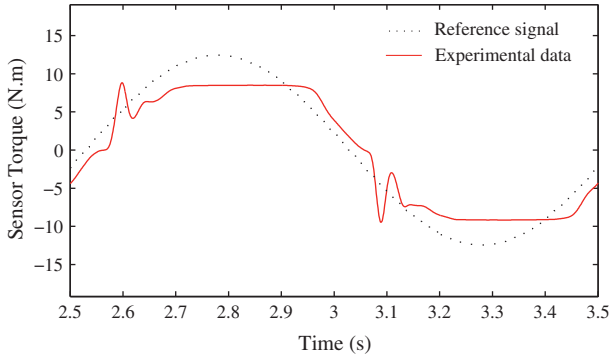

Fig. 13. Sensor torque, τ_d, for a sine wave excitation signal.

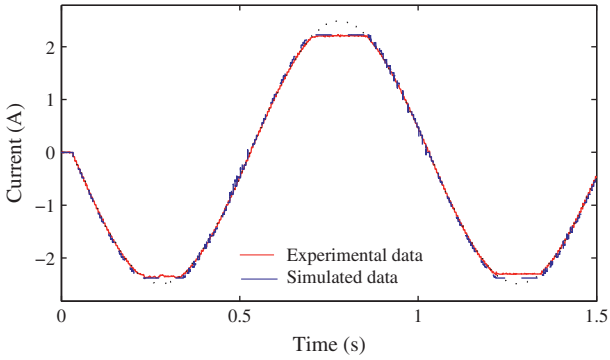

Fig. 15. Amplifier current, i_a, for a sine wave reference.

The tuned parameters of the model are presented in Table C.1. The tuning of the saturation limits of the voltage is addressed in Section 4.3.

4.1.2. Tuning of the motor friction parameters

Having found the optimal parameters for the amplifier, the following optimization is that of the friction parameters of the motor. The available data for the motor are the angle θ_m and the angular velocity ω_m. The sine wave reference with an amplitude of 2/3 of full scale is used. As a sine wave contains only one frequency, the influence of each friction parameter is more easily spotted. Here, the tuned parameters are $\alpha'_1,\ \alpha'_2,\ \alpha'_3$ for each rotational direction and σ_0 for the motor. The best results are obtained by tuning the parameters with respect to the motor angular velocity. Fig. 16 shows the experimental and simulated angular velocity of the motor and Fig. 17 shows the experimental and simulated angle of the motor.

The fits are of 95.4% for the motor angle and of 76.41% for the motor angular velocity. Although this last fit is not as high as that of the amplifier or the motor angle, the motor dynamics are well matched. Table C.2 shows the values of the tuned parameters.

4.1.3. Tuning of the gearbox friction parameters

Finally the friction parameters of the gearbox are adjusted. As for the motor, these parameters are $\alpha_1^+,\ \alpha_1^-,\ \alpha_2^+,\ \alpha_2^-,\ \alpha_3^+,\ \alpha_3^-$ and σ_0. Figs. 18 and 19 show the experimental and simulated torque of the sensor when using the sine wave reference and the random square wave. The values of the tuned parameters are compiled in Table C.3. The fit is of 88.8% for the sine wave reference and of 82.2% for the square wave reference. These results demonstrate that the model represents with high accuracy the dynamics of the driver's force feedback system when the steering wheel is blocked. The gearbox torque, that is the most important parameter of the model, is especially well represented.

4.2. Free steering wheel

When the steering wheel is free (i.e. the driver is not holding it) and a reference current is demanded, the steering wheel begins to turn and rapidly reaches a maximum rotational velocity. This velocity is a little lower than the no-load speed of the motor without the gearbox, as the geared motor has to overcome friction in the gearbox. The amplifier and the DC motor models presented in this paper explain this operating mode. When a reference current i_{dap} is given by the DAP, first this current is maintained between both saturation bounds as stated in Eq. (1). Then, the voltage V_a necessary to keep the motor current i_a equal to the reference current i_{ref} is calculated using Eq. (2) or Eq. (3) depending on the sign of i_{ref}. Since the motor has no load, the maximum current that can be drawn by the motor is the current necessary to overcome the friction forces, i_f. In that particular situation, V_a, obtained from Eq. (2b) or Eq. (3b), is equal to V_{sat}^+. Looking now at Eq. (4), the motor angular velocity ω_m which is the only remaining unknown, must be constant and equal to the no load speed as the rest of the variables are constants as explained above. Fig. 20 shows the current of the motor while Fig. 21 shows the angular velocity of the motor during a test in which a constant reference current of 0.64 A is applied to the steering wheel that is free.

The comparison between the experimental and the simulated data demonstrates that the model is accurate enough to represent this operating mode. The transient is not very well represented by the model but it has almost no impact on the accuracy as it is very fast. However the steady state is well matched for both the motor current and the motor angular velocity. The fit is not given as it would not be interesting in this case. Table C.1 shows the satura-

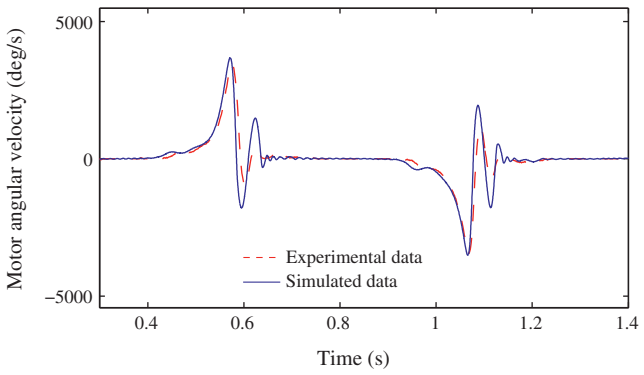

Fig. 16. Motor angular velocity, ω_m, for a sine wave reference.

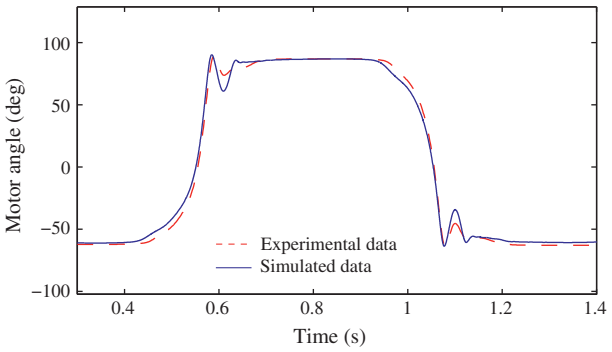

Fig. 17. Motor angle, θ_m, for a sine wave reference.

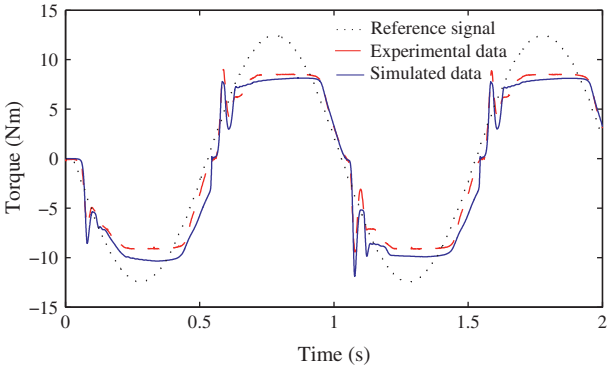

Fig. 18. Gearbox torque, τ_g, for a sine wave reference.

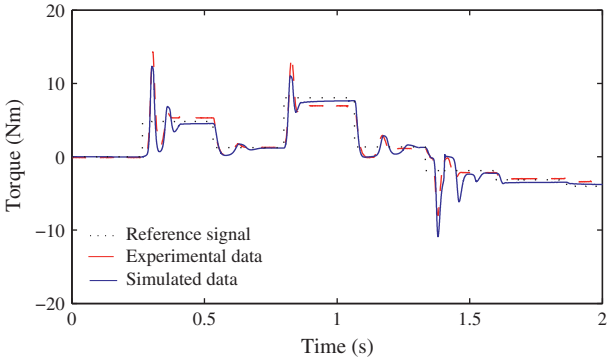

Fig. 19. Gearbox torque, τ_g, for a square wave reference.

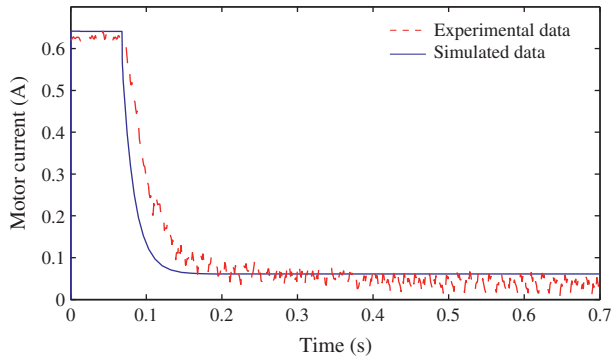

Fig. 20. Motor current, i_a.

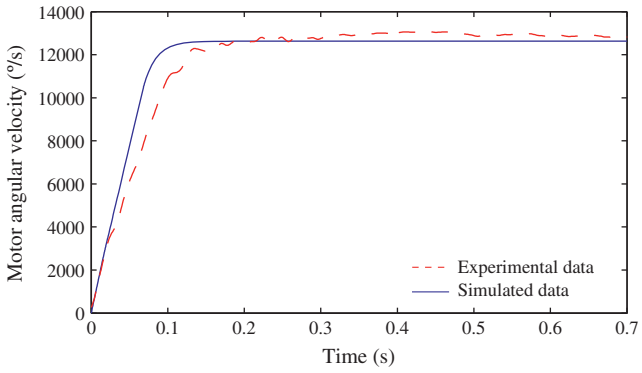

Fig. 21. Motor angular velocity, ω_m.

tion limits of the voltage V_a and Table 1 shows the maximum speed reached by the geared motor for both real and simulated data.

4.3. Held steering wheel

A schematic of this operating mode is shown in Fig. 4. In this last test, the driver turns the steering wheel in both rotational directions while the amplifier attempts to follow its reference current. In the locked and free steering wheel tests, the motor is always motoring, therefore absorbing electrical energy and producing mechanical work. Nevertheless in this test, the torque applied by the driver to the steering wheel can lead to a regenerative behaviour, where the current is inverted and fed back to the amplifier. In quadrants 2 and 4, i.e. when the motor acts as a generator, the amplifier actively controls the motor current. If the Counter Electromotive Force (CEMF) is low, power is dissipated within the amplifier in order to maintain the current equal to its reference. In this case there is no regenerative effect of power being fed back to the power supply. If the CEMF created becomes too high, the amplifier begins to return the excess of energy to the power supply via internal diodes.

Table 1
Real and simulated rotational velocity.

$\omega^{max}_{m,real}$ (°/s)	12,780
$\omega^{max}_{m,simulated}$ (°/s)	12,631

Considering the operating modes of the driver's force feedback system, the motor can generate energy in three different situations. In the first case, the reference current is zero and the driver turns the steering wheel in any direction. As a torque is normally applied to the motor, this situation does not normally occur. In the second case, the driver turns the steering wheel in the direction that opposes the motor's reference current (differing from zero). Finally in the third case, the driver turns the steering wheel in the same direction as the motor's reference current at a velocity higher than the no-load speed. In the three cases, the generated CEMF creates a torque that goes against the driver's movement.

The Simulink model employed in this section is presented in Fig. 22. In order to complete the optimization of the model parameters, a last experimental test is realized. A constant reference current is applied to the motor while the driver turns the steering wheel in both directions increasing for each movement its rotational velocity. The objective is that the motor actuates in quadrants 2 and 4. During this test, the torque in the steering wheel (τ_d), the gearbox angle (θ_g), the motor angle (θ_m), the motor voltage (V_a) and the motor current (i_a) are recorded. To run the simulation, two inputs are necessary: the current applied to the motor (i_a) and the driver's torque acting on the steering wheel (τ_d). Whilst the reference current applied to the motor is known, the driver's torque has to be obtained using a PI controller as there is no torque sensor. The PI error is the difference between the known experimental velocity and the simulated velocity of the steering wheel. The PI coefficients K_p and K_d are tuned until the simulated velocity of the steering wheel matches the experimental velocity (recorded previously). They are compiled in Table C.4. The comparison between the experimental and the simulated data presented in Fig. 23, shows that the match is very good. The fit is of 98.2%.

The angle of the gearbox during the experimental test is shown in Fig. 24. As for the gearbox velocity, the simulated gearbox angle (or the steering wheel angle), follows its reference with high accuracy and the fit is of 91.4%.

After that, the friction parameters of the motor are finely tuned to match the simulated data to the experimental data. The three basic variables of the motor model, ω_m, i_a and V_a stated in Eq. (4), are presented in Fig. 25–27. The respective values of the fit are 88.6%, 92.6%, 92.6%.

Finally the friction parameters of the gearbox are finely tuned to match the experimental and simulated data. Once all the model parameters have been optimized, the driver's torque of the model

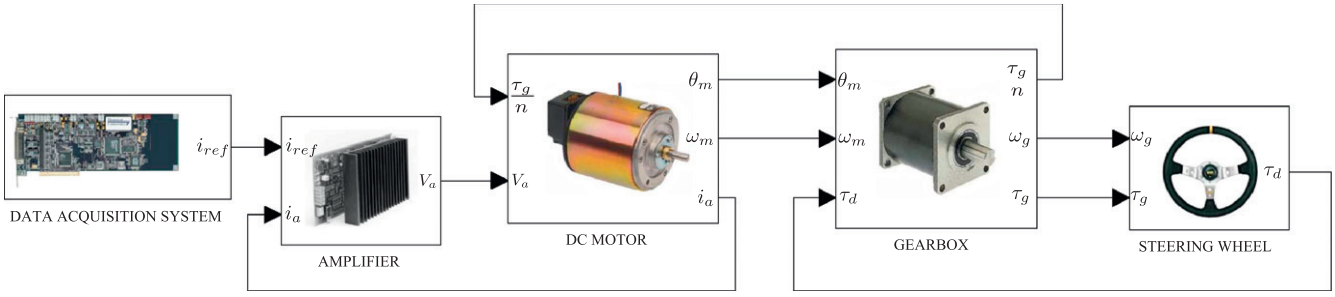

Fig. 22. Simulink model of the driver's torque feedback system for the steering wheel held.

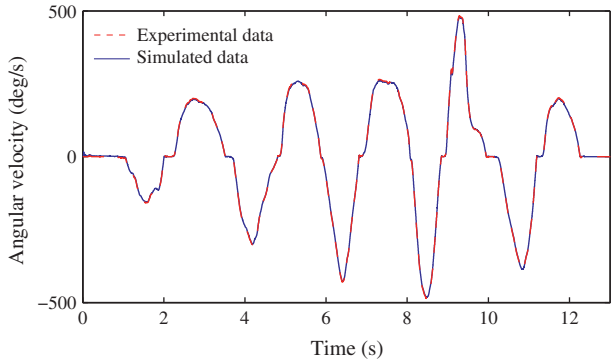

Fig. 23. Angular velocity of the gearbox, ω_g.

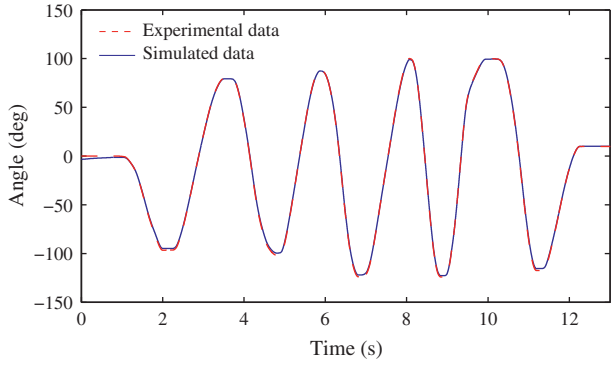

Fig. 24. Angle of the gearbox, θ_g.

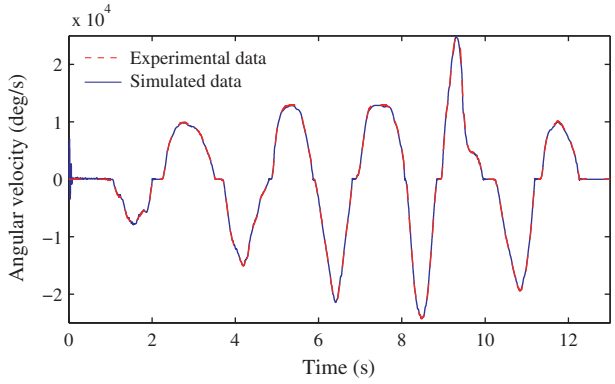

Fig. 25. Motor velocity, ω_m.

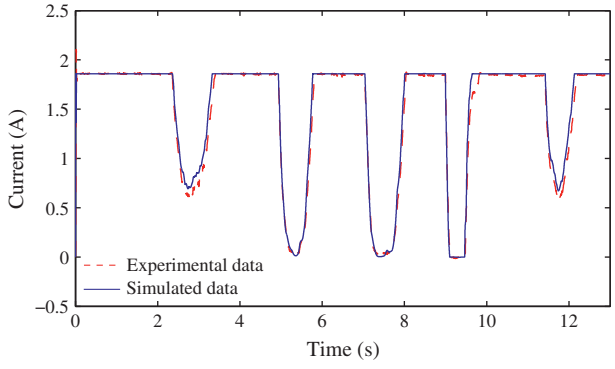

Fig. 26. Motor current, i_a.

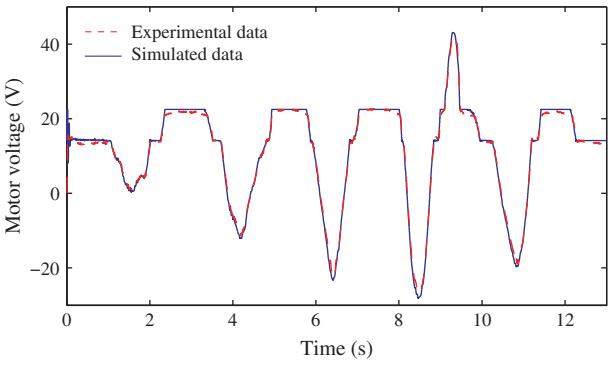

Fig. 27. Motor voltage, V_a.

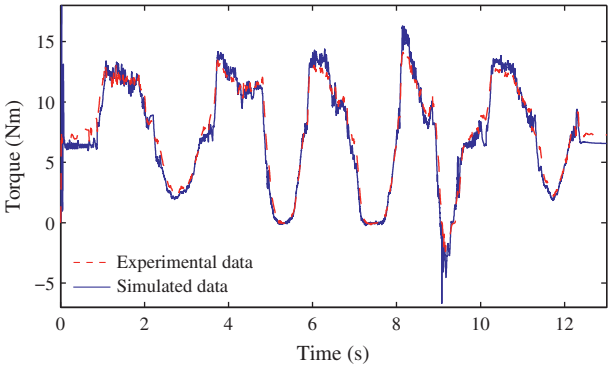

Fig. 28. Driver's torque, τ_d.

matches well the experimental driver's torque recorded during the test, as can be seen in Fig. 28. Although the fit, 45.7%, is lower than the previous fits, it demonstrates that when a motor torque is applied to the system and the angular velocity of the steering wheel is known, the driver's torque of the model is very similar the experimental driver's torque. The results obtained in this section demonstrate that the model, not only matches the dynamics of the real system with the steering wheel blocked or free, but also represents with high accuracy the dynamics of the system when both input torques, the motor torque and the driver's torque, are applied to the system.

5. Conclusions

In this paper, a general approach to model accurately amplifier–motor–gearbox assemblies has been developed. This approach that takes into account backlash, flexibility, friction for stiction and sliding, identification procedures, is applicable to a wide range of amplifier–motor–gearbox assemblies. It has been presented through an example: the modelling of a low cost driver's torque feedback system of a steer-by-wire system that uses a two stage planetary gearbox, a coreless PMDC motor and a four quadrant linear amplifier. All the parameters of this model have a direct physical significance thus making easier the identification procedures. The amplifier has been modelled as a current controller which takes into account the four quadrant operating modes. Then, the PMDC motor has been modelled as a resistor, a coil and a CEMF in series. Friction within both the motor and the gearbox has been taken into account by using a modification of the LuGre model that allows friction to be considered as load-dependent. Backlash and flexibility within the gearbox have been considered together using a fifth order polynomial for each rotational direction.

Table A.1
Specification of the DC motors – electrical data.

Rotor	Ironless
Direction of rotation	Reversible
Nominal voltage	30 VDC
Nominal speed	2120 rpm
Nominal load	100×10^{-3} Nm
No-load speed	2300 rpm
Voltage constant, k_v	10.5 mV/rpm ± 10%
Torque constant, k_m	100×10^{-3} Nm/A ± 10%
Terminal resistance, R_a	7.6 Ω ±8%
Rotor inductance at 1 kHz, L_a	3 mH (typical)

Table B.1
Identified friction parameters with no load applied.

Rotation	Positive	Negative
$F_{c,no\ load}$ (10^{-5} Nm)	2.4	0.34
$F_{s,no\ load}$ (10^{-6} Nm)	2.58	0.84
$v_{s,no\ load}$ (rad/s)	3.49	7.93
$\sigma_{2,no\ load}$ (10^{-6} Nm/rad/s)	1	1.15

Table B.2
Gearbox elasticity parameters.

Rotation	Positive	Negative
k_{g1} (Nm/rad)	5	1
k_{g2} (Nm/rad^3)	2e5	9e5
k_{g3} (Nm/rad^5)	3e8	18e8

Table B.3
System component inertias.

	Inertia (10^{-6} kg m^2)
J_m	22
J_1	40.5
J_2	294
J_{sw}	17,789

Table C.1
Amplifier parameters.

Param.	Value	Unit	Comment
V_{sat}^+	22.5	V	Positive saturation of the motor voltage
V_{sat}^-	−22.5	V	Negative saturation of the motor voltage
i_{sat}^+	2.23	A	Positive saturation of the motor current
i_{sat}^-	−2.38	A	Negative saturation of the motor current
k_1	30,000	Ω	Coeff. when $\lvert i_{ref}\rvert < \lvert i_a\rvert$
k_2	10,000	Ω	Coeff. when sign (i_{ref}) ≠ sign (i_a)

Table C.2
Motor parameters.

Param.	Value	Unit	Comment
σ_0	5	Nm	Stiffness of the britsles
α_1'	0.2	(Nm)$^{-1}$	Load dependent coeff.
α_2'	0.3	(Nm)$^{-1}$	Load dependent coeff.
α_3'	1e−5	s/Nm	Load dependent coeff.
v_s	0.174	s	Stribeck velocity

Comparisons between simulations and experimental data for three typical driving situations show that the model represents the system's dynamics with high accuracy. Future work will focus on the design of a controller employing a torque observer to compensate the gearbox drawbacks using the model developed in this paper.

Table C.3
Gearbox parameters.

Param.	Value	Unit	Comment
n	50	–	Gearbox ratio ω_{in}/ω_{out}
b_g	0.1	Nm/s	Coeff. of the viscous term of the gearbox
σ_0	3000	Nm	Stiffness of the britsles
α_1^+	0.4	(Nm)$^{-1}$	Load dependent coeff.
α_2^+	0.5	(Nm)$^{-1}$	Load dependent coeff.
α_3^+	1e−5	s/Nm	Load dependent coeff.
α_1^-	0.05	(Nm)$^{-1}$	Load dependent coeff.
α_2^-	0.06	(Nm)$^{-1}$	Load dependent coeff.
α_3^-	1e−5	s/Nm	Load dependent coeff.
v_s	43.48	s	Stribeck velocity

Table C.4
PI controller parameters.

Param.	Value	Unit	Comment
k_p	200	N	Proportional coeff. of the PI controller
k_i	150	N	Integral coeff. of the PI controller

Acknowledgements

The authors thank the Spanish Ministry of Science and Innovation and ERDF funds through the grant TRA2009-09314 for its support in this research.

Appendix A. Specification of the DC motors – electrical data

See Table A.1.

Appendix B. Identification results

See Table B.1, B.2, B.3.

Appendix C. Tuned parameters of the driver's force feedback system model

See Table C.1, C.2, C.3, C.4.

References

[1] Nordin M, Gutman PO. Controlling mechanical systems with backlash – a survey. Automatica 2002;38:1633–49.
[2] Swevers J, Al-Bender F, Ganseman CG, Prajogo T. An integrated friction model structure with improved presliding behavior for accurate friction compensation. IEEE Trans Autom Control 2000;45:675–86.
[3] Canudas de Wit C, Olsson H, Aström KJ, Lischinsky P. A new model for control of systems with friction. IEEE Trans Autom Control 1995;40:419–25.
[4] Armstrong-Hélouvry B, Dupont P, Canudas de Wit C. A survey of models, analysis tools and compensation methods for the control of machines with friction. Automatica 1994;30:1083–138.
[5] Menon Jr K. Control of low velocity friction and gear backlash in a machine tool feed drive system. Mechatronics 1999;9:33–52.
[6] Márton L, Lantos B. Control of mechanical systems with stribeck friction and backlash. Syst Control Lett 2009;58:141–7.
[7] Wernholt E, Gunnarsson S. Nonlinear identification of a physically parameterized robot model. In: 14th IFAC symposium on system identification, Newcastle, Australia; 2006. p. 143–8.
[8] Yih P, Gerdes JC. Modification of vehicle handling characteristics via steer-by-wire. IEEE Trans Control Syst Technol 2005;13(6):965–76.
[9] Bianchi N, Bolognani S, Dai PrT M, Tomasini M, Peretti L, Zigliotto M. The steering effect. IEEE Ind Appl Mag 2008;14:40–8.
[10] Iyasere E, Black J, Kinstle M, Post B, Wagner J, Dawson D. A real time reconfigurable steering simulator for system design studies. In: Proceedings of the 2007 American control conference, vols. 1–13, New York, USA; 2007. p. 3760–6.
[11] Bajçinca N, Cortesão R, Hauschild M. Robust control for steer-by-wire vehicles. Auton Robots 2005;19:193–214.

[12] Heitzer D, Seewald A, Development of a fault tolerant steer-by-wire steering system. SAE International 2004-21-0046.
[13] Verschuren R, Duringhof H. Design of a steer-by-wire prototype. SAE International 2006-01-1497.
[14] Gualino D, Adounkpe IJ. Force-feedback system design for the steer-by-wire: optimisation and performance evaluation. in: Proceedings of the IEEE ITSC, Toronto, Canada; 2006. p. 181–7.
[15] Katsura S, Matsumoto Y, Ohnishi K. Modeling of force sensing and validation observer for force control. IEEE Trans Ind Electron 2007;54: 530–8.
[16] Dohring ME, Lee E, Newman WS. A load-dependent transmission fricton model: theory and experiments. In: IEEE international conference on robotics and automation, vol. 3; 1993. p. 430–6.